



ILL: 97848591

Call v.64-102(1960-1998)

Number:

Location:

Maxcost: 50.00IFM

DateReq: 11/29/2012 Yes

Date Rec: 11/29/2012 No

Borrower: CNR Conditional

Request Type:

Source: FSILLSTF

LenderString: *CLZ,COC,COF,CDF,COR

OCLC Number: 1681052

Affiliation:

Staff Email: ncarill@ucar.edu

Billing Notes:

Title: The journal of physical chemistry.

Uniform

Title:

Author:

Edition:

Imprint: Easton, Pa. : American Chemical Society, 1952 1996

Article: Clapp "Frequency-dependent optical constants of water ice obtained directly from aerosol extinction spectra"

Vol: 99

No.: 17

Pages: 63176326

Date: April 1995

Dissertation:

Verified: WorldCat CODEN: JPCHAX Desc: 45 v. : Type: Serial, Internet Resource 0022-3654

Borrowing Please email article copy requests to ncarill@ucar.edu THANKS. CCLS Courier: NCAR/BOULER; CNR is Notes: nonprofit and doesn't charge. (maxCost: \$50)

ShipTo: Library-Interlibrary Loan-Nat Ctr Atmospheric Research/3090 Center Green Drive/Boulder CO US 80301

E-delivery

Addr: 303-497-1170

Ship Via: courier/Library Rate

ShipVia: courier/Library

Return To:

Interlibrary Loan
Adams State University Library
Alamosa, CO 81101

Ship To:

Library-Interlibrary Loan-Nat Ctr Atmospheri
3090 Center Green Drive
Boulder CO US 80301



ILL: 97848591

Lender: CLZ

NeedBy: 12/29/2012

Borrower: CNR

Req Date: 11/29/2012

OCLC #: 1681052

Patron: Steven Massie

Author:

Title: The journal of physical chemistry.

Article: Clapp "Frequency-dependent optical constants of water ice obtained directly from aerosol extinction spectra"

Vol.: 99

No.: 17

Date: April 1995

Pages: 63176326

Verified: WorldCat CODEN: JPCHAX Desc: 45 v. : T

Maxcost: 50.00IFM

Due Date:

Lending Notes:

Bor Notes: Please email article copy requests to ncarill@ucar.edu THANKS. CCLS

Frequency-Dependent Optical Constants of Water Ice Obtained Directly from Aerosol Extinction Spectra

M. L. Clapp and R. E. Miller*

Department of Chemistry, University of North Carolina, Chapel Hill, North Carolina 27599

D. R. Worsnop

Center for Chemical and Environmental Physics, Aerodyne Research Inc., Billerica, Massachusetts 10821

Received: August 23, 1994; In Final Form: February 7, 1995[Ⓞ]

We report here a new approach for determining frequency-dependent real and imaginary components of the refractive index of crystalline solids directly from the observation of the infrared spectra of the corresponding aerosols. The interplay between scattering and absorption observed in large ($>0.5\text{-}\mu\text{m}$ -radius) particles allows us to properly scale the imaginary component, determined from the absorption spectrum of small (around $0.3\text{-}\mu\text{m}$ -radius) aerosols, using calculations based on the Mie scattering theory. Once the imaginary indices are properly scaled, the corresponding real indices are determined through a Kramers–Kronig analysis. The method is applied to the study of water ice aerosols, and comparisons with previous measurements confirm that the method is sound and accurate. Reported here is a detailed study of the temperature dependence of the refractive index of ice. Experiments are reported over the temperature range from 130 to 210 K, which includes the region of interest for the study of polar stratospheric clouds (PSC's).

Introduction

The influence of clouds on the behavior of planetary atmospheres has recently been underscored by the determination that polar stratospheric cloud (PSC) particles play a critical role in the formation of the Antarctic stratospheric ozone hole.^{1–6} Due to the large surface-to-volume ratio associated with these cloud particles, they can provide an important site for heterogeneous chemistry. In the Jovian atmosphere, for example, cloud surfaces may serve as catalytic sites for ortho-to-para hydrogen conversion.⁷ On a global scale, the interaction between cloud particles and incident solar radiation is a critical factor determining planetary heat balance.^{7–11} Along with an appreciation for the importance of these factors in planetary atmospheres has come increased attention on the characterization of these atmospheric particles, as well as on the associated gas–surface interactions and chemistry.

Our understanding of the influences of aerosols on atmospheric behavior is still quite limited. The link between polar ozone depletion and PSC's is a case in point, given that the composition of PSC's is still the subject of some debate.¹² It is now generally accepted that PSC's exist in two forms, namely, type I and type II.¹³ Type I clouds are formed at temperatures somewhat above the frost point of water ice aerosols. Under these conditions, the most stable solid phase is nitric acid trihydrate (NAT),^{12,14–19} although the possibility that other hydrates of nitric acid might exist in the stratosphere has not been eliminated.¹² In addition, the role that the background sulfate aerosols play in the formation of PSC's is still poorly understood.^{10,20–22} At lower ambient temperatures, background aerosols can grow by condensation of water vapor, giving rise to larger, predominantly water ice, particles (type II PSC's).¹³ Although considerable progress has recently been made in understanding the heterogeneous chemistry associated with thin films of these ices,^{4,23–30} many open questions remain concerning the composition, optical properties,¹³ and chemistry^{5,31,32} of the actual aerosols.

In the present study, we have developed a new approach for obtaining optical properties of crystalline materials, based upon

the study of laboratory-generated aerosols. The approach is quite versatile and is used here to determine and study the temperature dependence of the optical constants of water ice. This study clears up several open questions relative to the large differences in the optical constants obtained by various workers,^{33–42} providing a unifying picture that reconciles these data. In addition, we provide the first definitive refractive index data for water ice at stratospherically relevant temperatures (near 190 K). This is important given that the present study clearly shows that the temperature dependence of the optical properties of ice is quite significant.

Given the importance of water in the above context and the immense scientific effort that has been expended in the study of its various phases, it is not surprising that a large number of studies have been reported on the infrared spectroscopy of its ices, under a variety of conditions.^{33–40,43–52} The infrared spectrum of ice is dominated by what can be crudely assigned as strong O–H stretch absorptions in the $3\text{-}\mu\text{m}$ region and a somewhat weaker and broader band around $12\text{ }\mu\text{m}$, due to librational motions in the crystal. Several weaker bands are also observed at intermediate wavelengths, associated with the O–H bending vibrations, as well as overtone and combination bands of lower frequency lattice modes. As pointed out by Sivakumar et al.,⁴⁹ however, the strong coupling between the various vibrational and librational modes of this solid makes assignment of the features in the spectrum to specific molecular vibrations difficult and not an entirely useful concept. This conclusion was reached by carrying out a series of isotopic dilution experiments, which help to better define the nature of the inter- and intramolecular couplings.⁵² The strong mixing of the normal modes is a primary source of the broadening observed in the spectrum, particularly in the O–H stretch region. Another broadening source is the proton disorder in the solid, which destroys the symmetry of the crystal and allows all vibrations to be infrared active. At the low pressures of interest in the present study (1 bar and lower), only two phases of crystalline ice are stable, namely, ice I_h and I_c .³⁴ The structural differences between these two forms of ice are subtle and result in no detectable change in the infrared spectrum.^{36,46}

The infrared absorption spectra of bulk ice have primarily been obtained by recording transmission spectra of cryogenically

[Ⓞ] Abstract published in *Advance ACS Abstracts*, April 1, 1995.

deposited ice films. To convert the corresponding spectra into real and imaginary components of the refractive index ($n + ik$), care must be taken to quantify the exact magnitude of the absorption by the precise measurement of the film thickness.^{53–55} Once the thickness of the film is measured, the imaginary component can be determined from the absorption coefficient α , where $k = \alpha\lambda/4\pi$. The corresponding real portion of the complex refractive index is related to the phase velocity of light in the bulk material and is not directly probed by this type of spectroscopic measurement. Nevertheless, once the frequency-dependent k values are determined, the corresponding frequency dependence of n can be obtained using the Kramers–Kronig transform.^{35,56} Although the problems associated with film thickness determination have been minimized,^{53–55} the necessity of growing the films on an infrared transparent substrate can result in several difficulties. For example, reflections at the interfaces can be difficult to account for, since the simple recording of a blank or reference spectrum of the bare substrate only partially corrects for these losses since reflections at the substrate/vacuum interface can be different from those at the substrate/film/vacuum interface.⁵⁷ Also, the need for samples of rather large thickness often makes it difficult to ensure that the sample is uniform in both structure and composition. Crystalline defects cannot be avoided, and amorphous samples⁵⁴ must be subjected to repeated annealing to reach even moderate degrees of crystallinity. In severe cases, the substrate can prevent the nucleation of some crystals,¹⁹ while other amorphous deposits cannot be annealed due to severe cracking of the sample itself.⁵⁵

Another approach for obtaining refractive index data of bulk samples involves the measurement of the absolute reflectivity of a sample.⁵⁸ When used in conjunction with the Fresnel equations, this technique enables the direct determination of n in regions of low k .^{35,56} At wavelengths where k is nonnegligible, the reflected power is a sensitive function of both optical constants, and a self-consistent set of n and k can be determined through the use of the Kramers–Kronig transform.^{35,56}

The most recent review of the frequency-dependent refractive index data for water ice is that of Warren.³⁶ In this review, he compiled a wide range of data from the infrared to the ultraviolet on the absorption of polycrystalline ice, I_h . By choosing the most consistent data sets for the imaginary component of the refractive index in the temperature range 213–273 K and scaling them to agree at their respective end points, he obtained sufficient data to perform a Kramers–Kronig transformation to determine the corresponding real indices. For the midinfrared region of the spectrum considered here, the imaginary indices of Schaaf and Williams³⁵ were used. These data were obtained by reflection measurements from a block of ice at 266 K. The resulting data of Warren have been used in a number of modeling situations, including PSC's at 190 K^{13,59} and the reflection spectra of icy asteroid surfaces at 100 K,⁶⁰ both of which are well outside the temperature range of the refractive index measurements.³⁶

The second data set that is relevant to the present study is that of Bergren et al. (BSSR),³⁷ who measured n and k in the 3- μm region at 150 K using thin film transmission measurements. BSSR took extra care to account for reflection losses in their samples, which many researchers had not done previously.^{41,46} In addition, Toon et al.⁴² have recently reported refractive indices at 163 K over a frequency interval similar to that studied here. These data are again quite different from the Warren data and are much more similar to that of BSSR. Finally, Tsujimoto et al.⁶¹ have discussed the optical properties of I_h at 180, 150, and 77 K. These researchers report very little

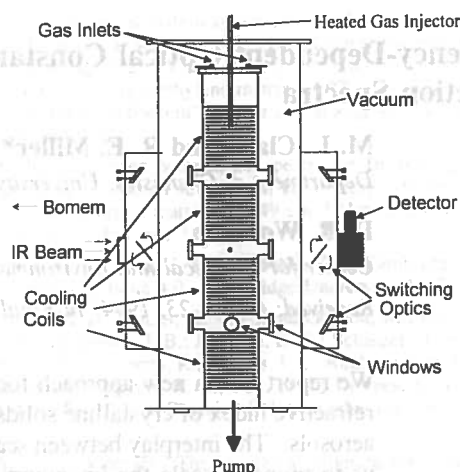


Figure 1. Schematic diagram of the aerosol cell used in the present experiments. The cell consists of a copper cylinder 80-cm long by 10-cm diameter with four separate cooling regions. The cell is thermally isolated from its surroundings by short pieces of thin wall stainless steel of the same diameter at each end. Aerosols homogeneously nucleate in the top section and flow down the tube to the outlet. The particles are probed by FT-IR through one of three sets of windows shown in the drawing.

difference in retrieved refractive index values over this wide range of temperature. However, as shown in the following sections, the differences between the Warren,³⁶ BSSR,³⁷ and Toon et al.⁴² sets can be completely understood in terms of the temperature dependence of the optical properties of water ice.

Experimental Section

The aerosols of interest in the present study are generated in an 80-cm-long, 10-cm-diameter cylindrical copper cell, shown schematically in Figure 1. Four separate cooling coils are used to control the temperature of the three observation regions. Cold nitrogen gas flows through the cooling coils, and the temperature of each zone is monitored by copper/constantan thermocouples. Temperature control is achieved using an electronic feedback circuit that regulates the current through four corresponding sets of heating tape wrapped around the outside of the tube. In this way, each zone can be maintained at a different temperature and controlled to ± 1 K. The entire cell is wrapped with several layers of aluminized mylar to reduce the heat load from ambient radiation.

The aerosol spectra are recorded using a Bomem DA3.02 FT-IR operating over the range 700–5000 cm^{-1} . The beam from the interferometer is steered through the cell by a set of transfer optics and focused onto a mercury cadmium telluride (MCT) detector. The steering optics shown in Figure 1 were used to direct the FT-IR beam through the desired set of ZnS windows. Typically, 50 interferograms at 2- cm^{-1} resolution were added to produce a final spectrum. This raw spectrum was referenced against an empty cell spectrum recorded just prior to the filling the cell. A second empty cell spectrum was recorded after the cell was evacuated to ensure that the spectra were not compromised by condensation on the windows. This procedure was then repeated under a variety of conditions to record a series of spectra as a function of particle size and temperature.

The aerosols of interest are formed by the homogeneous nucleation of water vapor in a nitrogen buffer gas. A MKS flow controller is used to meter the flow of nitrogen through a water bubbler to make the desired gas mixture, typically 1% water in nitrogen for the present experiments. The composition of the mixture was determined by recording a high-resolution

spectrum of the gas in the cell at room temperature. After flowing from the bubbler, the gas mixture enters the top of the copper flow cell where the nitrogen cools by collisions with the walls, in turn cooling the water vapor, resulting in supersaturation of the water and the formation of an aerosol. The flow conditions and temperature profiles are adjusted to minimize turbulent and convective flow. Light scattering from a helium neon laser is used to visually monitor the motion of the particles. Laminar flow conditions were used throughout this study, as determined by the fact that the particles are all flowing parallel to the cell axis. The pump and fill rates of the gases are kept constant and equal in order to maintain the desired total pressure, which is normally in the range 100–300 Torr, corresponding to a water vapor partial pressure of 1–3 Torr. This dynamic equilibrium gives a stable distribution of particles over the entire time scale of the experiment.

In previous studies,^{62–64} we have shown that the particle size distribution is a strong function of the supersaturation at the nucleation point and, hence, the temperature at which nucleation occurs. In general, we find that at low temperatures the gas is highly supersaturated and many critical nuclei are formed, resulting in the formation of small particles. At higher temperatures, the supersaturation is lower, and the nucleation rate is correspondingly slower. As a result, fewer particles form and, given the fact that the vapor reservoir is the same, they are able to grow to larger size. Once the gas phase is depleted, growth stops and the particles cool to the ambient temperature controlled by the cell walls. In the present study, we take advantage of this temperature dependence of the nucleation and growth processes to control the aerosol size distribution and, hence, that relative importance of the scattering and absorption contributions to the infrared spectrum. Since nucleation and growth occur in the top section of the cell, the temperature of this zone controls the size distribution. Once formed, the particles flow down the cell into the observation zones which can be maintained at temperatures different from the nucleation zone. In this way, we can independently control the size distribution and the observation temperature.

At the flow rates (4 SLM (standard liters per minute)) and total pressures (100–300 Torr) used in this study, the typical laminar flow velocity of the gas down the cell is approximately 2 cm/s. As a result, the residence time of the aerosols in the cell is approximately 40 s. Since most measurements were made using the bottom set of windows, the time between nucleation and observation of the aerosols was around 30 s. This was much longer than the temperature equilibration of the gas stream with the wall of ≤ 1 s. Since this equilibration time is short with respect to the transit time from one observation zone to the next, the aerosols effectively remain in equilibrium with the cell walls at all times. High-resolution spectroscopic studies of gas-phase species, such as ammonia, under these flow conditions show that the rotational temperature is in equilibrium with the walls at each point in the flow.

Present Methodology

In previous studies of laboratory aerosols generated as discussed above,^{62–64} we have shown that, if frequency-dependent refractive index data are available, the aerosol spectra can be modeled over a wide range of particle sizes using only two parameters, namely, the median size (r_{med}) and the width (or standard deviation, σ) of a log-normal size distribution.⁶⁵ The question we now pose is “Do the aerosol spectra contain enough information to independently determine the frequency dependence of the refractive index?”. One of the strengths of such an approach is that we can control the relative importance

of the real and imaginary components of the refractive index in the aerosol spectra by controlling the size of the particles. Large particles are effective at scattering the infrared light and the associated spectra are strongly dependent upon the real component of the refractive index, n , while absorption dominates the spectra of smaller particles with radii less than the wavelength of the light. At first sight, it appears as if the problem is intractable given that there are two unknowns at each wavelength (n and k), in addition to the size distribution parameters for each spectrum. Fortunately, this heavily over-parameterized picture can be greatly simplified if we take advantage of the fact that the spectra of small particles are primarily dependent on the imaginary component of the refractive index (k), which is directly proportional to the absorbance.^{66,67} In this respect, small-particle spectra can be quite similar to transmission spectra of a thin film, effectively defining the relative k values across the entire frequency range of measurement. An important difference from the thin film case is that the aerosols are unsupported. As a result, reflection losses only occur at the windows, and since these are not changed by the presence of the aerosol, they are completely accounted for by recording an empty cell reference spectrum. An additional advantage of studying unsupported aerosols is that the crystals grow in the absence of any influence from a substrate.

An apparent difficulty with the approach is that we do not know the effective “thickness” of our sample, which is determined by the number density of aerosol particles in the cell. As a result, the scaling of the “ k spectrum” determined from the small aerosol absorption is arbitrary. Nevertheless, the small particle spectrum does define the relative magnitudes of the adopted k 's over the frequency range of interest. Thus, within a single scaling parameter, we have determined the frequency dependence of k . In a conventional thin film experiment, measurements of the thickness would effectively be used to determine this absolute scaling. Although we cannot make an *a priori* determination of the analogous parameter for the present case, we do have the advantage that the scattering spectra associated with the larger particles depend upon both the real and the imaginary components. For example, consider what will happen if an improperly scaled initial k spectrum is used to generate the frequency-dependent n values using a subtractive Kramers–Kronig routine. The resulting set of complex refractive indices will have the incorrect absolute values of both n and k and, thus, will not give the correct ratio of scattering to absorption in the larger aerosol spectra, calculated using the Mie theory.^{65,66,68} Therefore, by introducing an extra fitting parameter, namely, the scaling factor for k , the scattering aerosol spectrum can be fit using the k spectrum and the two parameters associated with the log-normal size distribution. The uniqueness of the fit results from the fact that the size distribution changes the relative importance of scattering and absorption in the calculated spectrum in a very different way than the scaling of k . Indeed, in all of the experiments discussed below, the fits to these three parameters all converged well within excellent confidence limits. On each iteration, the newly scaled k values from the small-particle spectrum were used in conjunction with the Kramers–Kronig routine to obtain a new set of n values. These new indices were then used as input to a Mie scattering code along with the two parameters of the size distribution. Once a fit is obtained, the refractive index data set can be further tested by performing a two-parameter fit (r_{med} and σ) to other scattering spectra with very different contributions from absorption and scattering.

Although the small-particle spectra are dominated by absorption, which is proportional to the imaginary index, this

proportionality constant is dependent upon the real index, which in turn is dependent on frequency. This effect is clearly going to be most pronounced in the region of the resonances, due to the dispersion in the real refractive index. In general, however, this is a second-order effect that can easily be corrected by a second iterative step. In particular, we take the refractive indices determined using the method discussed above to fit the small particle spectrum originally used as input for the k values. Since the associated Mie calculation includes this dispersion effect, which was originally ignored, it will result in differences between the experimental small-particle spectrum and the result of the fit. For the case of water, the largest differences were in the 3- μm region where the dispersion is strongest. In fact, due to the breadth of the absorption band in this region, the effect is moderately strong. We used the difference between the calculated and observed spectrum to correct the original input k spectrum and repeat the first iterative procedure. The differences resulting from this extra iteration step were small but did improve the overall quality of the fits to the large particle spectra. All of the results shown below have been corrected in this way.

A few previous attempts have been made at determining refractive indices directly from aerosol measurements. Meehan and Miller⁶⁷ used small-particle absorption spectra and angular scattering measurements to determine n and k for monodisperse colloidal silver bromide particles at a few ultraviolet frequencies. Eiden⁶⁹ discussed the possibility of using angular light scattering measurements coupled with polarization selectivity to determine complex refractive indices for lognormal distributions of particles. Avery and Jones⁷⁰ have reported an attempt to measure the index of refraction of coal particles at one frequency using angular scattering measurements. Finally, Milham, et al.⁷¹ have determined the complex refractive indices of orthophosphoric acid aerosols from 7 to 14 μm using the infrared extinction spectrum of an aerosol cloud for which the size distribution of the particles was independently determined. Knowing the size distribution, the k values at each wavelength were interactively adjusted, using a Kramers–Kronig routine to obtain n and Mie scattering to calculate the spectrum. This latter method is most similar to the present one, although it was complicated by the fact that particle sizing is necessary. For the cryogenic and volatile aerosols considered here, independent sizing can present significant problems since the particles are in equilibrium with the vapor. As a result, in the process of pulling the particles into a sizing apparatus, the conditions can change enough to dramatically alter the size distribution. Therefore, the fact that the present method uses only the optical measurements to determine the refractive index data is a distinct advantage.

The Kramers–Kronig transform^{66,72–75} makes use of the fact that k and n are integrally related, which is to say that if one is known at all frequencies, the other can be calculated directly. Since the true Kramers–Kronig relation requires that either n or k be known at all frequencies, the subtractive Kramers–Kronig relation⁷⁶ is often used:

$$n(\nu) = n(\nu_0) + \frac{2(\nu^2 - \nu_0^2)}{\pi} P \int_0^{\infty} \frac{\nu' k(\nu') d\nu'}{(\nu^2 - (\nu')^2)(\nu_0^2 - (\nu')^2)} \quad (1)$$

P signifies that the Cauchy principle value of the integral must be taken and $n(\nu_0)$ is the real index at a wavelength inside the integration region, which is known from some other measurement. This value has been referred to as the “anchor point” of the integration.⁷⁷ Given $k(\nu)$ and $n(\nu_0)$, we can use this integral

to compute the corresponding set of real index values. In the subtractive Kramers–Kronig procedure, all real index values are determined in relation to the anchor point, which helps to reduce the effects of truncating the integration and using only a finite set of $k(\nu)$. An error in the value of the anchor point will cause a shift in the n values by a constant amount, while the overall shape of the frequency-dependent curve will be preserved.⁷⁶

In the present study, the refractive indices were calculated using a modified version of a subtractive Kramers–Kronig transform FORTRAN program written by Palmer, Williams, and Budde.⁷⁶ Ideally, the anchor point in this calculation should lie near the middle of the integrated range to minimize the effects of absorptions that are outside the range of interest.^{57,78} However, since the k values for ice are rather large in this region of the spectrum, the corresponding n values depend strongly on the scaling of k . As a result, this is a poor choice for the location of the anchor point. On the other hand, ice does not absorb strongly at frequencies above the O–H stretch band, all the way up to 40,000 cm^{-1} .³⁶ By positioning the anchor point well outside the absorption region, to the blue of the O–H stretch peak, the real index at the anchor point becomes insensitive to changes in the absorption spectrum. Calculations were performed with the anchor point at a number of frequencies in this range to establish that the resulting data were insensitive to this variable.

The value of the real index at the anchor point was determined from the published data at 4000 cm^{-1} . In this region, the various data sets are in good agreement, even though they were carried out at very different temperatures. This is consistent with the discussion of the previous paragraph, which argues that at frequencies that are far removed from strong absorption features, the real index should be insensitive to changes in the absorption features. The real index reported by Warren at 4000 cm^{-1} is 1.226, corresponding to 267 K, while the value of Bertie et al.⁴⁶ at 100 K is 1.236. This small difference in the real refractive index in this region as a function of temperature underscores the above point. For the present purpose, we chose a value of 1.232 for the anchor value of the real index at 4000 cm^{-1} , since the temperature range of interest here falls midway between these two results. Over the temperature range of interest here, the change in this anchor value will be very small, and we found that the refractive index data sets reported in the following section were insensitive to such small differences. As a result, all of the data sets reported below were determined using the same value for the anchor point, namely, 1.232.

The Mie calculations referred to above were carried out using a version of the Bohren and Huffman⁶⁶ FORTRAN code, modified to average over a log-normal distribution of sizes. While the Mie theory is strictly valid only for spheres, there is ample evidence to suggest that the sensitivity of the scattering to shape is often lost when averaging over a range of particle sizes, shapes, and orientations.^{79,80} Perry et al.⁸¹ determined that the Mie theory can adequately describe the scattering behavior of salt cubes up to a size parameter (ratio of the particle size to the wavelength of light) of about 3. For all of the experiments reported here, the size parameters are far smaller than this limit. In addition, Pope et al.⁷⁹ observed that the angular intensity of light scattered from ammonia ice aerosols could be quite well described by the Mie theory up to a size parameter of approximately 7, even when visual inspection of the particles revealed them to be nonspherical. The primary exception to this rule occurs when the real component of the refractive index is near zero and the imaginary portion is equal

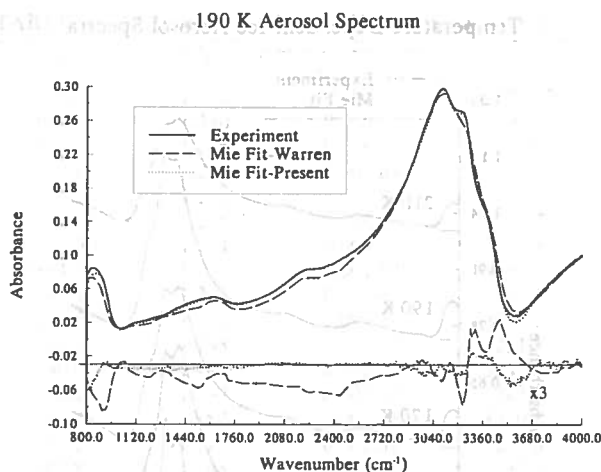


Figure 2. Infrared spectrum of an ice aerosol at 190 K. The dashed line is a fit to the data using the Mie theory in conjunction with the refractive index data of Warren, yielding $r_{\text{med}} = 1.05 \mu\text{m}$ and $\sigma = 0.26$. The dotted line is the Mie fit using the refractive index data obtained from the present study at 190 K, yielding $r_{\text{med}} = 0.79 \mu\text{m}$ and $\sigma = 0.40$. The residuals of the fit are shown below the spectrum. The latter have been multiplied by a factor of 3 and offset by -0.03 for clarity, such that the solid line represents a residual of zero.

to the square root of two. Under these conditions, particles much smaller than the wavelength of light can show highly shape-dependent absorptions due to the excitation of surface resonance or Fröhlich modes.^{66,82-89} We have discussed these modes and their effect on the infrared spectrum of ammonia ice aerosols in detail in another publication.⁶⁴ For water ice, this condition is not met, and given the size range considered here, the Mie theory should be an excellent model for the aerosol spectra. Therefore, the use of the Mie theory should in no way compromise the results reported here.

Another caveat of the spectral modeling in this approach needs to be addressed, and this is that when the spectra are only weakly scattering, the uniqueness of the log-normal size distribution is a problem. For small particle sizes and relatively narrow standard deviations, similar extinction spectra can be obtained with a range of particle size distributions. However, as the mean size of the particles becomes larger, and scattering becomes more prominent in the spectra, the problem disappears, and the fits converge to a unique distribution. For this reason, we focused our attention on fitting larger particle spectra ($r_{\text{med}} > 0.5 \mu\text{m}$) that showed enough scattering in the spectrum to guarantee uniqueness.

Experimental Results

We begin this discussion by comparing in Figure 2 an aerosol spectrum at 190 K with the result of a Mie calculation based upon the refractive index data of Warren. The agreement is clearly only semiquantitative, as illustrated by the residuals given directly below the spectra. The primary differences occur in the regions of strong absorption, where the Warren data do not reproduce either the shape or the intensity of the $3\text{-}\mu\text{m}$ and $12\text{-}\mu\text{m}$ bands. This is consistent with the previous work of Callagan et al.,⁹⁰ who reported difficulty in reproducing the "doublet" at the peak of the $3\text{-}\mu\text{m}$ band in their experimentally generated aerosol spectra. The Warren data gave even poorer agreement with aerosol spectra recorded at lower cell temperatures, leading us to the conclusion that the refractive index is strongly dependent upon temperature and that the existing data are inappropriate for use in the study of PSC's.

Figure 3 shows an expanded view of the $3\text{-}\mu\text{m}$ region for a series of typical spectra recorded with the nucleation region

Non-Scattering, Small Particle Spectra - $3\text{-}\mu\text{m}$ band

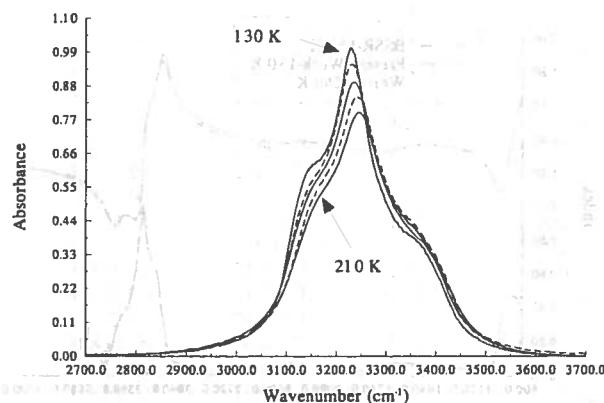


Figure 3. Expanded view of the O-H stretch region of typical small ice particles as a function of temperature. The peak intensities have been scaled in relation to their relative peak values of the imaginary refractive index. Spectra are shown at 20 K intervals from 210 to 130 K.

Scattering Aerosol Spectrum and Mie Fit at 130 K

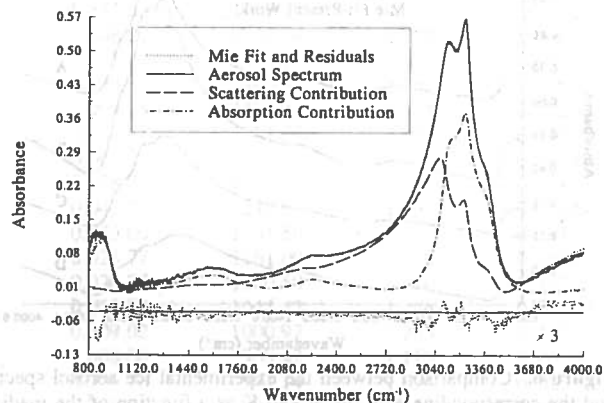


Figure 4. Comparison between the experimental ice aerosol spectrum at 130 K and the Mie fit, using the refractive indices determined here for 130 K. The absorption and scattering contributions to the band are also shown, indicating that the doublet at $3 \mu\text{m}$ results from the interplay between these two contributions. The residuals of the fit are shown below the spectrum. The latter have been multiplied by a factor of 3 and offset by -0.04 for clarity, such that the solid line represents a residual of zero.

maintained at 130 K, resulting in the formation of small particles, and varying the temperature of the lower observation port over the range 130–210 K. Close examination of the absorption curves shows that the O-H band broadens slightly and shifts to higher frequency as the temperature is increased. The broadening of the band is also associated with an overall decrease in the peak absorption intensity. Although these qualitative trends have been noted previously in the literature,⁹¹ there has been no systematic and quantitative study aimed at determining the temperature dependence of the real and imaginary refractive index except for the work of Tsujimoto et al. Since this work is in disagreement with other reports and shows very little change in index with temperature, we do not consider these data valid in light of the present discussion.

Consider for a moment a spectrum recorded at an observation temperature of 130 K. As discussed above, this absorption spectrum can be converted into a k spectrum, within a scaling factor. The resulting k spectrum can then be used to determine the frequency dependence of n using the Kramers-Kronig method discussed above. Mie calculations can then be carried out and the calculations compared with the experimental spectrum of a scattering aerosol at the same temperature. The

Comparison of Refractive Indices

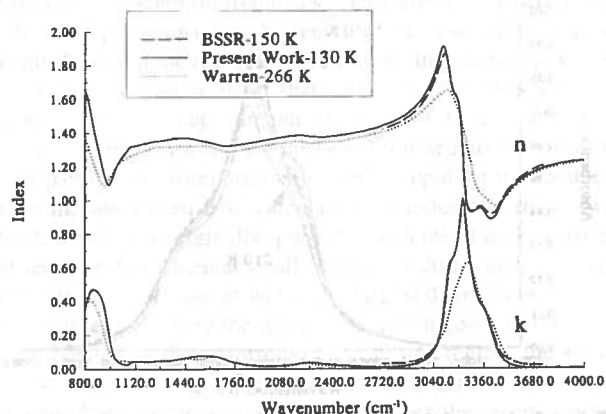


Figure 5. Comparison between the refractive index data of Warren³⁶ at 266 K, the present study at 130 K, and the BSSR³⁷ data at 150 K.

Ice Aerosols at 180 K

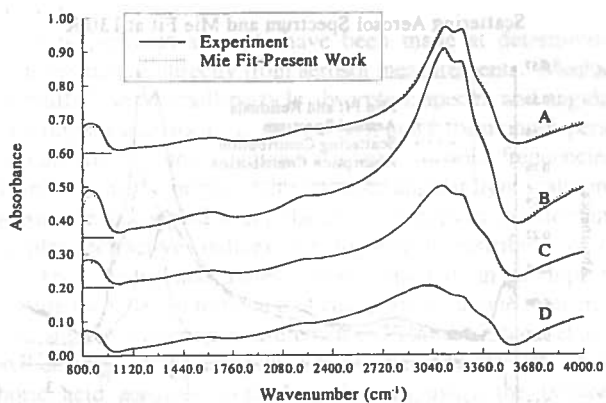


Figure 6. Comparison between the experimental ice aerosol spectra and the corresponding Mie fits at 180 K as a function of the median size of the aerosols. A single set of refractive index data is used in all three fits, and the resulting size distributions are (A) $r_{\text{med}} = 0.65 \mu\text{m}$ and $\sigma = 0.36$, (B) $r_{\text{med}} = 0.77 \mu\text{m}$ and $\sigma = 0.33$, (C) $r_{\text{med}} = 0.82 \mu\text{m}$ and $\sigma = 0.37$, and (D) $r_{\text{med}} = 1.2 \mu\text{m}$ and $\sigma = 0.35$. The spectra are shown offset in absorbance, with the zero absorbance line for each spectrum indicated by the corresponding line at low frequency.

latter spectrum can then be fit by varying the k scaling and the two parameters defining the particle size distribution. Figure 4 shows the resulting fit at 130 K after applying the scattering correction as discussed above. The agreement is clearly excellent, reproducing the doublet in the O–H stretching region, as well as the structure of the weak bands at longer wavelengths. The only region where there is significant disagreement between the experimental and calculated spectra is near 800 cm^{-1} . This discrepancy can be explained in terms of truncation errors in the Kramers–Kronig integration. Since the long-wavelength cutoff of our spectra is very close to the tail of the $12\text{-}\mu\text{m}$ band and ice has very strong absorptions at frequencies below this cutoff, truncation errors are introduced into the real indices at the edge of the frequency range. Toon et al.⁴² have reported similar problems, even though their measurements extended to 500 cm^{-1} .

Figure 4 also shows the separate contributions to the spectrum from scattering and absorption, obtained from the Mie calculations. It is clear from this presentation of the data that the doublet in the O–H stretch region results from the interplay between these two contributions. It is the fact that the scattering aerosol spectrum is thus strongly dependent on both n and k in these regions that provides us with the sensitivity we need to constrain the scaling in k and then determine n . Unless the

Temperature Dependent Ice Aerosol Spectra

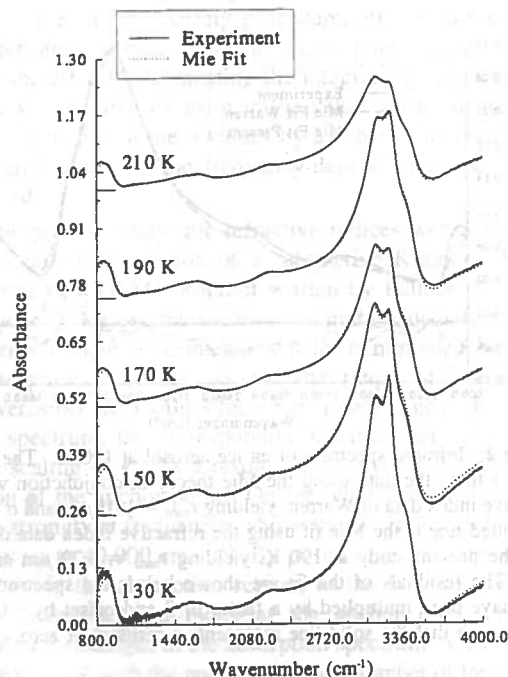


Figure 7. Series of scattering aerosol spectra and Mie fits as a function of temperature. The size distributions determined from these fits are at 210 K, $r_{\text{med}} = 0.5 \mu\text{m}$ and $\sigma = 0.33$; at 190 K, $r_{\text{med}} = 0.65 \mu\text{m}$ and $\sigma = 0.36$; at 170 K, $r_{\text{med}} = 0.68 \mu\text{m}$ and $\sigma = 0.32$; at 150 K, $r_{\text{med}} = 0.69 \mu\text{m}$, $\sigma = 0.36$; and at 130 K, $r_{\text{med}} = 0.49 \mu\text{m}$ and $\sigma = 0.40$. These distributions show no systematic trend since the flow rates and pressures were different for each case. The zero absorbance lines have been indicated below each spectrum as in Figure 6.

Refractive Index of Water Ice

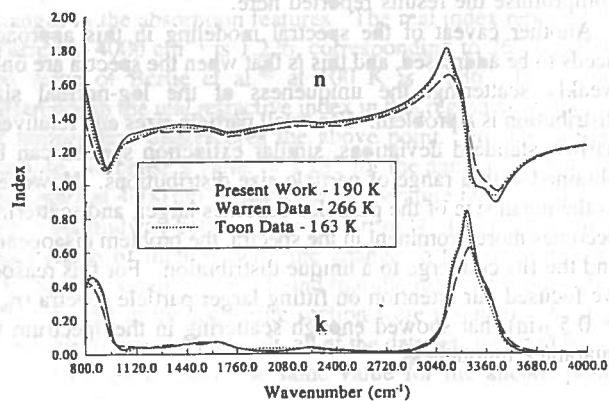


Figure 8. Comparison between the refractive indices determined from the present study at 190 K (solid lines) with those of Warren (dashed lines) and Toon et al. (dotted lines). This serves to illustrate the fact that the Warren data are inappropriate for use in describing PSC's.

detailed shape and magnitude of the real and imaginary components of the refractive indices are properly determined the detailed structure in these spectra cannot be reproduced, as illustrated by the results in Figure 2.

To illustrate the magnitude of the temperature dependence of these optical constants, we show in Figure 5 the refractive indices obtained from the present study at 130 K, compared with that of Warren at 266 K. In the O–H stretching region, the k values for the two sets of data differ by nearly a factor of 2. On the other hand, the present data are in excellent agreement with the BSSR data at 150 K, although the latter are limited to only the O–H stretch region.

Once the refractive index data are determined from the above procedure, it can be further tested by fitting other aerosol spectra

TABLE 1: Refractive Indices of Water Ice at 190 K

cm ⁻¹	<i>n</i>	<i>k</i>	cm ⁻¹	<i>n</i>	<i>k</i>	cm ⁻¹	<i>n</i>	<i>k</i>
4000.00	1.232	0.001 77	3307.37	0.986	0.520 27	2520.65	1.386	0.011 18
3980.58	1.230	0.000 79	3297.72	0.991	0.563 31	2480.15	1.381	0.012 80
3961.30	1.226	0.000 90	3290.01	1.003	0.601 97	2441.57	1.376	0.015 09
3940.08	1.224	0.001 66	3282.29	1.019	0.640 34	2401.07	1.371	0.17 59
3920.80	1.221	0.000 97	3274.58	1.043	0.690 45	2360.57	1.367	0.021 49
3901.51	1.218	0.000 59	3270.72	1.061	0.713 64	2320.07	1.364	0.024 83
3880.30	1.214	0.000 71	3266.87	1.080	0.738 98	2281.50	1.364	0.029 81
3861.01	1.210	0.001 54	3263.01	1.106	0.764 80	2241.00	1.367	0.033 44
3841.73	1.207	0.000 41	3259.15	1.136	0.785 99	2200.50	1.373	0.032 21
3820.51	1.202	0.001 54	3255.29	1.167	0.806 74	2160.00	1.375	0.026 17
3801.23	1.198	0.000 55	3251.44	1.207	0.824 74	2121.43	1.373	0.019 57
3780.01	1.192	0.002 28	3247.58	1.247	0.832 87	2080.93	1.368	0.016 13
3760.73	1.187	0.001 90	3243.72	1.285	0.838 16	2040.43	1.362	0.012 59
3741.44	1.182	0.001 58	3239.87	1.327	0.843 00	2001.87	1.356	0.011 48
3720.23	1.175	0.002 37	3236.01	1.372	0.838 32	1961.37	1.349	0.011 52
3700.94	1.168	0.002 02	3232.15	1.412	0.824 96	1920.87	1.343	0.013 13
3681.65	1.160	0.000 89	3228.29	1.449	0.809 31	1880.37	1.336	0.015 75
3660.44	1.150	0.000 63	3224.44	1.481	0.788 38	1841.79	1.331	0.018 96
3641.15	1.138	0.000 57	3220.58	1.506	0.766 55	1801.29	1.324	0.023 53
3600.51	1.110	0.006 18	3209.01	1.562	0.704 40	1720.29	1.312	0.045 79
3581.22	1.094	0.009 72	3201.29	1.587	0.667 58	1681.71	1.319	0.059 86
3560.01	1.073	0.016 57	3189.72	1.613	0.625 74	1641.21	1.328	0.069 57
3540.72	1.051	0.023 72	3174.29	1.652	0.583 56	1600.71	1.339	0.068 76
3521.44	1.029	0.036 30	3158.86	1.702	0.541 29	1560.21	1.345	0.068 37
3500.22	1.001	0.053 03	3135.72	1.778	0.448 22	1521.64	1.350	0.066 60
3490.58	0.986	0.063 83	3104.86	1.798	0.271 29	1481.14	1.354	0.062 99
3484.80	0.978	0.069 12	3074.01	1.733	0.154 39	1440.64	1.357	0.056 50
3477.08	0.0964	0.081 55	3043.15	1.672	0.099 28	1400.14	1.358	0.052 81
3469.37	0.950	0.090 60	3027.72	1.646	0.080 87	1361.57	1.356	0.046 00
3461.65	0.938	0.109 48	3012.29	1.620	0.068 29	1321.07	1.351	0.042 84
3453.94	0.923	0.123 85	3000.72	1.608	0.058 83	1280.57	1.345	0.038 89
3446.22	0.909	0.147 89	2971.79	1.577	0.043 27	1240.07	1.337	0.038 64
3438.51	0.900	0.173 35	2950.58	1.557	0.033 00	1201.50	1.330	0.039 00
3430.79	0.895	0.199 01	2931.29	1.538	0.025 77	1161.00	1.320	0.038 80
3423.08	0.891	0.228 14	2910.08	1.523	0.020 75	1120.50	1.310	0.042 01
3407.65	0.901	0.281 44	2871.51	1.499	0.012 82	1041.42	1.266	0.026 88
3399.94	0.908	0.306 63	2850.29	1.486	0.009 02	1000.92	1.203	0.043 68
3392.22	0.919	0.326 71	2831.01	1.475	0.008 06	960.42	1.119	0.120 81
3384.51	0.930	0.349 21	2811.72	1.466	0.006 70	941.14	1.094	0.205 63
3376.79	0.941	0.362 33	2790.65	1.458	0.005 21	921.85	1.117	0.302 33
3369.08	0.951	0.378 92	2771.36	1.449	0.004 62	900.64	1.190	0.386 39
3361.37	0.959	0.390 19	2750.15	1.441	0.004 01	881.35	1.263	0.424 81
3353.65	0.965	0.407 16	2730.86	1.434	0.003 51	860.14	1.347	0.445 45
3345.94	0.973	0.417 76	2711.58	1.428	0.003 52	840.85	1.425	0.453 34
3338.22	0.975	0.435 02	2680.72	1.419	0.004 82	821.57	1.507	0.438 42
3330.51	0.980	0.451 12	2640.22	1.409	0.005 25	800.35	1.591	0.392 75
3322.79	0.981	0.470 51	2601.65	1.400	0.006 77			
3315.08	0.982	0.494 33	2561.15	1.393	0.009 11			

recorded at the same temperature, varying only r_{med} and σ . This is a useful test since spectra resulting from particles of different size will have very different admixtures of absorption and scattering. This is illustrated in Figure 6, which shows a series of spectra recorded at an observation temperature of 180 K, along with the Mie theory fits. As expected, the scattering contribution to the spectrum increases with increasing median particle size. The fact that these two parameter fits are excellent gives further confirmation of the data set determined using the procedure discussed above.

Complex refractive indices were determined using a large number of spectra recorded at 10 K intervals over the temperature range 130–210 K. Figure 7 shows a series of scattering spectra at 20 K intervals, along with the fit obtained using the refractive index data set determined for each temperature. The fits are clearly very good over the entire range of temperatures. Once again, all of these data sets were tested by two parameter fits to a wide range of spectra with different median particle sizes. Indeed, the ability to vary the observation temperature over a wide range is a powerful advantage of this technique, relative to the thin film method. In order to accurately constrain the magnitude of the k values determined from thin film work,

not only must the thickness be known precisely but it must also remain constant over the course of the experiment. This can be difficult for films at relatively high temperatures where the condensed species may have appreciable vapor pressure. For example, while two solid phases of acetylene are known to exist, refractive index data only exist for the low-temperature phase,⁹² due to the fact that the high vapor pressure of the high-temperature phase makes it difficult to maintain a film for long enough to acquire the necessary data. In the case of water, the adsorption and desorption kinetics have been well studied and indicate that evaporation of a water surface is quite rapid (> 10 monolayers/s) above 180 K.⁹³ In the present experiment, we form a stable distribution of aerosols over a wide temperature range by maintaining equilibrium between the gas and solid phases.

In view of its importance in the study of PSC's, the refractive index data determined at 190 K are shown in Figure 8. These data are also summarized at a limited number of wavelengths in Table 1. Once again, the results are compared with those of Warren at 266 K, illustrating the importance of the temperature dependence. The recent data of Toon et al.⁴² are also shown in the figure, with much better agreement because of the much

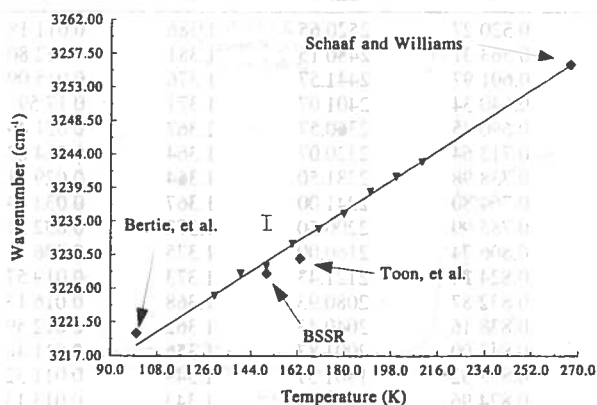
Peak Absorption Frequency vs. Temperature
for OH Stretch Region

Figure 9. Plot of the O–H stretch absorption frequency vs temperature. The data are shown with a least-squares fit which extrapolates well to the data of Schaaf and Williams³⁵ near the freezing point and the data of Bertie et al. at 100 K. Also shown are the peak absorption frequencies of Toon et al. and the BSSR data. The slope of this line is approximately $2.3 \text{ cm}^{-1}/10 \text{ K}$, which is in good agreement with the value of $2.2 \text{ cm}^{-1}/10 \text{ K}$ reported by Sivakumar et al.⁴⁹

closer temperatures of their experiment. A more complete listing of the refractive indices at any of the temperatures studied here is available from the authors either on disk or by Internet.

Consider again the 190 K scattering spectrum shown in Figure 2. The dotted lines in the figure, for both the spectrum and residuals, show the fit to the data using the refractive indices given in Figure 8 and Table 1. Clearly, these indices give a much better description of the spectrum than the higher temperature Warren data, except possibly at the low-frequency end point for the reasons discussed above. It is interesting to examine the size distributions and aerosol number densities determined from fitting this spectrum to the two sets of indices. The fit using the Warren refractive indices yields $r_{\text{med}} = 1.05 \mu\text{m}$, $\sigma = 0.26$, and ρ (number density) = 7×10^5 particles/ cm^3 , while the fit using the present indices yields $r_{\text{med}} = 0.79 \mu\text{m}$, $\sigma = 0.40$, and $\rho = 1.5 \times 10^6$ particles/ cm^3 . From this, it is clear that the errors associated with determining the size distributions and number densities based upon the high-temperature refractive index data are quite large. Since the size distribution and number density control such values as the total surface area and cloud column mass,^{13,94,95} correct values of the refractive index are vital if these parameters are to be calculated with confidence.

A question that we now wish to address is "Are the refractive indexes determined here consistent with what has been observed previously for bulk films?". The possibility exists that they may be different, due to the fact that either we are carrying out the measurements on small particles that behave differently from the bulk or we are making somewhat different crystals (in quality or structure) compared with those of the bulk. The comparisons of the actual n and k values in the figures above (Figures 5 and 8) are clearly very good, when the temperature dependence is taken into account. For additional comparisons, we consider two features of the O–H stretching band. Figure 9 shows a plot of the peak frequency of the O–H stretching band of the input k -value aerosol spectra, as a function of the temperature. There is clearly a linear temperature dependence that beautifully extrapolates between the data of Schaaf and Williams³⁵ (used by Warren³⁶) recorded near the freezing point and that of Bertie et al.⁴⁶ The slope of approximately $0.23 \text{ cm}^{-1}/\text{K}$ is in good agreement with the value of $0.22 \text{ cm}^{-1}/\text{K}$ reported in the Raman studies of Sivakumar et al.⁴⁹ in the temperature range of 60–150 K.

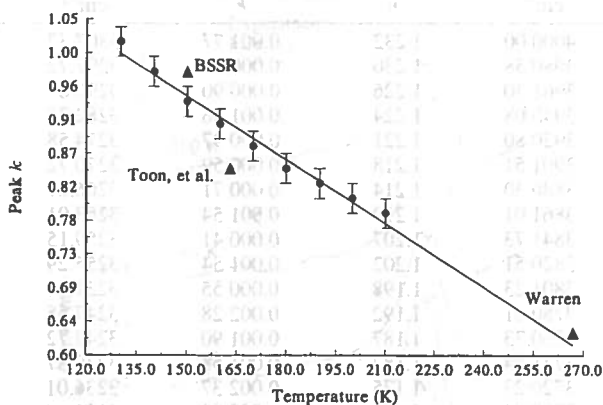
Peak k Value vs. Temperature
OH Stretch Region

Figure 10. Plot of the peak value of k in the O–H stretch region as a function of temperature. The linear fit to these data extrapolates well to the value determined by Warren at 266 K.³⁶ Also shown are the measurements of BSSR³⁷ and Toon et al.⁴² at their respective temperatures. The agreement between the published data and the present work is clearly excellent.

Figure 10 shows a plot of the value of k at the peak of the O–H band as a function of temperature determined from the present experiments. Once again, we observe a linear temperature dependence that interpolates well between the previous studies. This not only confirms that the present method produces quantitatively correct optical constants but also confirms that the aerosols we are producing are highly crystalline with the same structure as bulk ice. Therefore, this method provides an experimentally flexible alternative to traditional methods of refractive index determination. The present results serve to unify the available data sets on water ice and provide new data at temperatures of importance in the atmosphere. The differences between the various data sets appear to be primarily due to the strong temperature dependence of these optical constants.

It is interesting to note (see Figure 10) that the temperature dependence of the peak absorbance intensity in the O–H stretch region is much stronger than the corresponding dependence of the density of ice. Indeed, the latter changes by only 1% over the relevant temperature range,⁹⁶ while the peak absorbance changes by nearly a factor of 2. It is clear from this that the temperature dependence of the optical constants cannot be explained simply in terms of the change in the number of absorbers per unit volume. This is not unexpected, given the work of Rice and co-workers,^{37,49,50,97} which clearly shows that the shape of this band reflects the fact that the individual oscillators are strongly coupled by intermolecular interactions. The orientational anisotropy of these interactions in water ice is most likely an important contributing factor to this temperature dependence. These new data on the temperature dependence of these optical constants should therefore provide important new points of comparison with future theoretical calculations for ice.

Conclusions

We have presented a novel method for determining the frequency-dependent complex refractive indices of icy aerosols in the midinfrared region. This technique, which uses the extinction spectra of laboratory generated aerosols to constrain the imaginary complex refractive index values and a Kramers–Kronig analysis to determine the corresponding real indices, has been successfully applied to water ice particles as a function of temperature from 210 K to 130 K. The temperature

dependence of the absorption coefficient in the 3- μm region is observed to be strong, with the peak absorption increasing linearly with decreasing temperature, in coincidence with a corresponding narrowing of the band. These data provide a basis for understanding the differences that exist between various data sets that existed previously in the literature, such as those of Warren,³⁶ Bergen et al.,³⁷ and Toon et al.⁴² This strong temperature dependence of the ice spectrum indicates caution must be exercised in the use of optical constant from temperatures far from the point of interest, for instance, modeling PSC particles around 190 K with refractive index data from 266 K as has been done previously. The present study also provides the necessary data for use under a wide variety of planetary and cometary conditions.

Acknowledgment. We gratefully acknowledge support from the Planetary Atmospheres Program of NASA and the Upper Atmosphere Research Program of NASA. M.L.C. acknowledges the NASA Graduate Student Researchers Program for a Fellowship. We also thank K. Plamer (Westminster College, Fulton, MO) and J. Pearl (NASA-Goddard) for supplying us with their Kramers-Kronig FORTRAN codes and for helpful discussions, as well as S. Rice for making his tabulated ice refractive index data available to us. We are also grateful to M. Tolbert for providing us with preprints of her work on the refractive index of ice.

References and Notes

- (1) Solomon, S. *Rev. Geophys.* **1988**, *26*, 131.
- (2) Rossi, M. J.; Malhorta, R.; Golden, D. M. *Geophys. Res. Lett.* **1987**, *14*, 127.
- (3) Tolbert, M. A.; Rossi, M. J.; Golden, D. M. *Geophys. Res. Lett.* **1988**, *15*, 847.
- (4) Leu, M. T. *Geophys. Res. Lett.* **1988**, *15*, 851.
- (5) Granier, C.; Brassuer, G. *J. Geophys. Res., D: Atmos.* **1992**, *97*, 18015.
- (6) Zetzsch, C.; Behnke, W. *Ber. Bunsenges. Phys. Chem.* **1992**, *96*, 488.
- (7) West, R. A.; Strobel, D. F.; Tomasko, M. G. *Icarus* **1986**, *65*, 161.
- (8) Carlon, H. R. *Appl. Opt.* **1970**, *9*, 2000.
- (9) Plass, G. N.; Kattawar, G. W. *Appl. Opt.* **1971**, *10*, 738.
- (10) Charlson, R. J.; Wigley, T. M. L. *Sci. Am.* **1994**, 48.
- (11) Orton, G. S.; Appleby, J. F.; Martonchik, J. V. *Icarus* **1982**, *52*, 946.
- (12) Worsnop, D. R.; Fox, L. E.; Zahniser, M. S.; Wofsy, S. C. *Science* **1993**, *259*, 71.
- (13) Kinne, S.; Toon, O. B.; Toon, G. C.; Farmer, C. B.; Browell, E. V.; McCormick, M. P. *J. Geophys. Res.* **1989**, *94*, 16481.
- (14) Tolbert, M. A.; Koehler, B. G.; Middlebrook, A. M. *Spectrochim. Acta* **1992**, *48*, 1363.
- (15) Smith, R. H.; Leu, M. T.; Keyser, L. F. *J. Phys. Chem.* **1991**, *95*, 5924.
- (16) Hanson, D. R.; Mauersberger, K. *J. Phys. Chem.* **1988**, *92*, 6167.
- (17) Koehler, B. G.; Middlebrook, A. M.; Tolbert, M. A. *J. Geophys. Res., D: Atmos.* **1992**, *97*, 8065.
- (18) Iraci, L. T.; Middlebrook, A. M.; Wilson, M. A.; Tolbert, M. A. *Geophys. Res. Lett.* **1994**, *21*, 867.
- (19) Berland, B. S.; Haynes, D. R.; Foster, K. L.; Tolbert, M. A.; George, S. M.; Toon, O. B. *J. Phys. Chem.* **1994**, *98*, 4358.
- (20) Pueschel, R. F.; Snetsinger, K. G.; Goodman, J. K.; Toon, O. B.; Ferry, G. V.; Oberbeck, V. R.; Livingston, J. M.; Verma, S.; Fong, W.; Starr, W. L.; Chan, K. R. *J. Geophys. Res., D: Atmos.* **1989**, *94*, 11271.
- (21) Larsen, N. *Geophys. Res. Lett.* **1994**, *21*, 425.
- (22) Tolbert, M. A. *Science* **1994**, *264*, 527.
- (23) Toon, O.; Browell, E.; Gary, B.; Lait, L.; Livingston, J.; Newman, P.; Pueschel, R.; Russell, P.; Shoeberl, M.; Toon, G.; Traub, W.; Valero, F. P. J.; Selkirk, H.; Jordan, J. *Chem. Phys.* **1993**, *261*, 1136.
- (24) Drdla, K.; Turco, R. P.; Elliot, S. J. *Geophys. Res., D: Atmos.* **1993**, *98*, 8965.
- (25) Stephens, S.; Rossi, M. J.; Golden, D. M. *Int. J. Chem. Kinet.* **1986**, *18*, 1133.
- (26) Quinlan, M. A.; Reihls, C. M.; Golden, D. M.; Tolbert, M. A. *J. Phys. Chem.* **1990**, *94*, 3255.
- (27) Zhang, R.; Jayune, J. T.; Molina, M. J. *J. Phys. Chem.* **1994**, *98*, 867.
- (28) Hanson, D. R.; Ravishankara, A. R.; Solomon, S. *J. Geophys. Res., D: Atmos.* **1994**, *99*, 3615.
- (29) Elliot, S.; Cicerone, R. J.; Turco, R. P.; Drdla, K.; Tabazadeh, A. *J. Geophys. Res., D: Atmos.* **1994**, *99*, 3497.
- (30) Kolb, C. E.; Worsnop, D. R.; Zahniser, M. S.; Davidovits, P.; Hanson, D. R.; Ravishankara, A. R.; Keyser, L. F.; Lue, M.-T.; Williams, L. R.; Molina, M. J.; Tolbert, M. A. Laboratory Studies of Atmospheric Heterogeneous Chemistry in Current Problems. In *Atmospheric Chemistry; Barker, J. R., Ng, C.-Y., Eds.*; Wiley: New York, 1994.
- (31) Crutzen, P. J.; Muller, R.; Bruhl, C.; Peter, T. *Geophys. Res. Lett.* **1992**, *19*, 1113.
- (32) Brasseur, G. P.; Granier, C.; Walters, S. *Nature* **1990**, *348*, 626.
- (33) Irvine, W. M.; Pollack, J. B. *Icarus* **1968**, *8*, 324.
- (34) Bertie, J. E.; Whalley, E. *J. Chem. Phys.* **1964**, *40*, 1637.
- (35) Schaaf, J. W.; Williams, D. *J. Opt. Soc. Am.* **1973**, *63*, 726.
- (36) Warren, S. G. *Appl. Opt.* **1984**, *23*, 1206.
- (37) Bergren, M. S.; Schuh, D.; Sceats, M. G.; Rice, S. A. *J. Chem. Phys.* **1978**, *69*, 3477.
- (38) Ockman, N. *Adv. Phys.* **1958**, *7*, 199.
- (39) Giguere, P. A.; Harvey, K. B. *Can. J. Chem.* **1956**, *34*, 798.
- (40) Hornig, D. F.; White, H. F.; Reding, F. P. *Spectrosc. Acta* **1958**, *12*, 338.
- (41) Ikawa, S. I.; Maeda, S. *Spectrochim. Acta* **1968**, *24*, 655.
- (42) Toon, O. B.; Tolbert, M. A.; Koehler, B. G.; Middlebrook, A. M.; Jordan, J. *J. Geophys. Res., D: Atmos.* **1994**, *99*, 25631.
- (43) Devlin, J. P. *J. Chem. Phys.* **1992**, *96*, 6185.
- (44) Rowland, B.; Fisher, M.; Devlin, J. P. *J. Chem. Phys.* **1991**, *95*, 1378.
- (45) Dore, J. C. *J. Molec. Struct.* **1990**, *237*, 221.
- (46) Bertie, J. E.; Labbe, H. J.; Whalley, E. *J. Chem. Phys.* **1969**, *50*, 4501.
- (47) Dorsey, N. E. *Properties of Ordinary Water-Substance*; Reinhold: New York, 1940.
- (48) Franks, F. *Water: A Comprehensive Treatise Volume 7: Water and Aqueous Solutions at Subzero Temperatures*; Plenum: New York, 1982.
- (49) Sivakumar, T. C.; Rice, S. A.; Sceats, M. G. *J. Chem. Phys.* **1978**, *69*, 3468.
- (50) McGraw, R.; Madden, W. G.; Bergren, M. S.; Rice, S. A.; Sceats, M. G. *J. Chem. Phys.* **1978**, *69*, 3483.
- (51) Bertie, J. E.; Jacobs, S. M. *J. Chem. Phys.* **1977**, *67*, 2445.
- (52) Haas, C.; Hornig, D. F. *J. Chem. Phys.* **1960**, *32*, 1763.
- (53) Martonchik, J. V.; Orton, G. S.; Appleby, J. F. *Appl. Opt.* **1984**, *23*, 541.
- (54) Wood, B. E.; Roux, J. A. *J. Opt. Soc. Am.* **1982**, *72*, 720.
- (55) Roux, J. A.; Wood, B. E. *J. Opt. Soc. Am.* **1983**, *73*, 1181.
- (56) Palmer, K. F.; Williams, D. *Appl. Opt.* **1975**, *14*, 208.
- (57) Ribbergard, G. K.; Jones, R. N. *Appl. Spectrosc.* **1980**, *34*, 638.
- (58) Bell, E. E. *Handbuch der Physik*; Springer-Verlag: Berlin, 1967; Vol. 25/2a, p 1.
- (59) Meerkoetter, R. *Geophys. Res. Lett.* **1992**, *19*, 1351.
- (60) Wilson, P. D.; Sagan, C.; Thompson, W. R. *Icarus* **1994**, *107*, 288.
- (61) Tsujimoto, S.; Konishi, A.; Kunitomo, T. *Cryogenics* **1982**, *22*, 603.
- (62) Dunder, T.; Clapp, M. L.; Miller, R. E. *J. Geophys. Res., E: Planets* **1993**, *98*, 1213.
- (63) Dunder, T.; Miller, R. E. *J. Chem. Phys.* **1990**, *93*, 3693.
- (64) Clapp, M. L.; Miller, R. E. *Icarus* **1993**, *105*, 529.
- (65) Kerker, M. *The Scattering of Light and Other Electromagnetic Radiation*; Academic: New York and London, 1969.
- (66) Bohren, C. F.; Huffman, D. R. *Absorption and Scattering of Light by Small Particles*; Wiley: New York, 1983.
- (67) Meehan, E. J.; Miller, J. K. *J. Phys. Chem.* **1968**, *72*, 1523.
- (68) van de Hulst, H. C. *Light Scattering by Small Particles*; Wiley: New York, 1957.
- (69) Eiden, R. *Appl. Opt.* **1971**, *10*, 749.
- (70) Avery, R. K.; Jones, A. R. *J. Phys. D* **1982**, *15*, 1373.
- (71) Milham, M. E.; Frickel, R. H.; Embury, J. F.; Anderson, D. H. *J. Opt. Soc. Am.* **1981**, *71*, 1099.
- (72) Ohta, K.; Ishida, H. *Appl. Spectrosc.* **1988**, *42*, 952.
- (73) Goplen, T. G.; Cameron, D. G.; Jones, R. N. *Appl. Spectrosc.* **1980**, *34*, 657.
- (74) Phillips, R. T. *J. Phys. D* **1983**, *16*, 489.
- (75) Pearl, J.; Ngoh, M.; Ospina, M.; Khanna, R. *J. Geophys. Res.* **1991**, *96*, 17477.
- (76) Palmer, K. F.; Wood, B. E.; Roux, J. A. AEDC-TR-80-30, 1981 (AD-A094214).
- (77) Cameron, D. G.; Escolar, D.; Goplen, T. G.; Nadeau, A.; Young, R. P.; Jones, R. N. *Appl. Spectrosc.* **1980**, *34*, 646.
- (78) Goplen, T. G.; Cameron, D. G.; Jones, R. N. *Appl. Spectrosc.* **1980**, *34*, 652.
- (79) Pope, S. K.; Tomasko, M. G.; Williams, M. S.; Perry, M. L.; Doose, L. R.; Smith, P. H. *Icarus* **1992**, *100*, 203.
- (80) Holiand, A. C.; Draper, J. S. *Appl. Opt.* **1967**, *6*, 511.
- (81) Perry, R. J.; Hunt, A. J.; Huffman, D. R. *Appl. Opt.* **1978**, *17*, 2700.

(82) Steyer, T. R.; Day, K. L.; Huffman, D. R. *Appl. Opt.* **1974**, *13*, 1586.
 (83) Martin, T. P. *Phys. Rev. B: Condens. Matter* **1973**, *7*, 3906.
 (84) Hunt, A. J.; Steyer, T. R.; Huffman, D. R. *Surf. Sci.* **1973**, *36*, 454.
 (85) Luxon, J. T.; Montgomery, D. J.; Summitt, R. *Phys. Rev.* **1969**, *188*, 1345.
 (86) Martin, T. P. *Phys. Rev.* **1969**, *177*, 1349.
 (87) Fröhlich, H. *Theory of Dielectrics*; Clarendon: Oxford, 1958.
 (88) Hayashi, S. *Jpn. J. Appl. Phys.* **1984**, *23*, 665.
 (89) Fuchs, R. *Phys. Rev. B: Condens. Matter* **1975**, *11*, 1732.
 (90) Callaghan, R.; Lim, I. J.; Murdoch, D. E.; Sloan, J. J.; Donaldson, D. J. *Geophys. Res. Lett.* **1994**, *21*, 373.
 (91) Fox, J. J.; Martin, A. E. *Proc. R. Soc. London* **1940**, *A174*, 234.

(92) Khanna, R. K.; Ospina, M. J.; Zhao, G. *Icaurs* **1988**, *73*, 527.
 (93) Haynes, D. R.; Tro, N. J.; George, S. M. *J. Phys. Chem.* **1992**, *96*, 8502.
 (94) McDonald, G. D.; Thompson, W. R.; Heinrich, M.; Khare, B. N.; Sagan, C. *Icaurs* **1994**, *108*, 137.
 (95) Turco, R. P.; Whitten, R. C.; Toon, O. B. *Rev. Geophys. Space Phys.* **1982**, *20*, 233.
 (96) Hobbs, P. V. *Ice Physics*; Clarendon Press: Oxford, 1974.
 (97) Rice, S. A.; Bergren, M. S.; Belch, A. C.; Nielson, G. J. *Phys. Chem.* **1983**, *87*, 4295.
 JP9422506

Acknowledgment We gratefully acknowledge support from the Planetary Atmospheres Program of NASA and the Planetary Atmospheres Research Program of NASA, M. J. C. also acknowledges the NASA Graduate Student Research Program for support. We also thank L. Pagan (Westminster College) for her and J. Ford (NASA-Goddard) for supplying us with their Kramers-Kronig FORTRAN codes and for helpful discussions, as well as S. Rice for making us available to this project. This work was supported by grants from the National Science Foundation (ATM-93-01000) and the Planetary Atmospheres Program of NASA (ATM-93-01000).

References and Notes

1. J. J. Fox, *Proc. R. Soc. London*, **1940**, *A174*, 234.
 2. T. P. Martin, *Phys. Rev.*, **1969**, *177*, 1349.
 3. T. P. Martin, *Phys. Rev. B: Condens. Matter*, **1973**, *7*, 3906.
 4. A. J. Hunt, T. R. Steyer, and D. R. Huffman, *Surf. Sci.*, **1973**, *36*, 454.
 5. J. T. Luxon, D. J. Montgomery, and R. Summitt, *Phys. Rev.*, **1969**, *188*, 1345.
 6. H. Fröhlich, *Theory of Dielectrics*; Clarendon: Oxford, 1958.
 7. S. Hayashi, *Jpn. J. Appl. Phys.*, **1984**, *23*, 665.
 8. R. Fuchs, *Phys. Rev. B: Condens. Matter*, **1975**, *11*, 1732.
 9. R. Callaghan, I. J. Lim, D. E. Murdoch, J. J. Sloan, and D. J. Donaldson, *Geophys. Res. Lett.*, **1994**, *21*, 373.
 10. G. D. McDonald, W. R. Thompson, M. Heinrich, B. N. Khare, and C. Sagan, *Icaurs*, **1994**, *108*, 137.
 11. R. P. Turco, R. C. Whitten, and O. B. Toon, *Rev. Geophys. Space Phys.*, **1982**, *20*, 233.
 12. P. V. Hobbs, *Ice Physics*; Clarendon Press: Oxford, 1974.
 13. S. A. Rice, M. S. Bergren, A. C. Belch, and G. J. Nielson, *Phys. Chem.*, **1983**, *87*, 4295.
 14. M. J. C. Ospina, M. J. Khanna, and G. Zhao, *Icaurs*, **1988**, *73*, 527.
 15. D. R. Haynes, N. J. Tro, and S. M. George, *J. Phys. Chem.*, **1992**, *96*, 8502.
 16. L. Pagan and J. Ford, *Private Communication*.
 17. J. Ford and J. Pagan, *Private Communication*.
 18. S. A. Rice, *Phys. Chem.*, **1983**, *87*, 4295.
 19. National Science Foundation, Grant ATM-93-01000.
 20. National Science Foundation, Grant ATM-93-01000.
 21. National Science Foundation, Grant ATM-93-01000.
 22. National Science Foundation, Grant ATM-93-01000.
 23. National Science Foundation, Grant ATM-93-01000.
 24. National Science Foundation, Grant ATM-93-01000.
 25. National Science Foundation, Grant ATM-93-01000.
 26. National Science Foundation, Grant ATM-93-01000.
 27. National Science Foundation, Grant ATM-93-01000.
 28. National Science Foundation, Grant ATM-93-01000.
 29. National Science Foundation, Grant ATM-93-01000.
 30. National Science Foundation, Grant ATM-93-01000.
 31. National Science Foundation, Grant ATM-93-01000.
 32. National Science Foundation, Grant ATM-93-01000.
 33. National Science Foundation, Grant ATM-93-01000.
 34. National Science Foundation, Grant ATM-93-01000.
 35. National Science Foundation, Grant ATM-93-01000.
 36. National Science Foundation, Grant ATM-93-01000.
 37. National Science Foundation, Grant ATM-93-01000.
 38. National Science Foundation, Grant ATM-93-01000.
 39. National Science Foundation, Grant ATM-93-01000.
 40. National Science Foundation, Grant ATM-93-01000.
 41. National Science Foundation, Grant ATM-93-01000.
 42. National Science Foundation, Grant ATM-93-01000.
 43. National Science Foundation, Grant ATM-93-01000.
 44. National Science Foundation, Grant ATM-93-01000.
 45. National Science Foundation, Grant ATM-93-01000.
 46. National Science Foundation, Grant ATM-93-01000.
 47. National Science Foundation, Grant ATM-93-01000.
 48. National Science Foundation, Grant ATM-93-01000.
 49. National Science Foundation, Grant ATM-93-01000.
 50. National Science Foundation, Grant ATM-93-01000.
 51. National Science Foundation, Grant ATM-93-01000.
 52. National Science Foundation, Grant ATM-93-01000.
 53. National Science Foundation, Grant ATM-93-01000.
 54. National Science Foundation, Grant ATM-93-01000.
 55. National Science Foundation, Grant ATM-93-01000.
 56. National Science Foundation, Grant ATM-93-01000.
 57. National Science Foundation, Grant ATM-93-01000.
 58. National Science Foundation, Grant ATM-93-01000.
 59. National Science Foundation, Grant ATM-93-01000.
 60. National Science Foundation, Grant ATM-93-01000.
 61. National Science Foundation, Grant ATM-93-01000.
 62. National Science Foundation, Grant ATM-93-01000.
 63. National Science Foundation, Grant ATM-93-01000.
 64. National Science Foundation, Grant ATM-93-01000.
 65. National Science Foundation, Grant ATM-93-01000.
 66. National Science Foundation, Grant ATM-93-01000.
 67. National Science Foundation, Grant ATM-93-01000.
 68. National Science Foundation, Grant ATM-93-01000.
 69. National Science Foundation, Grant ATM-93-01000.
 70. National Science Foundation, Grant ATM-93-01000.
 71. National Science Foundation, Grant ATM-93-01000.
 72. National Science Foundation, Grant ATM-93-01000.
 73. National Science Foundation, Grant ATM-93-01000.
 74. National Science Foundation, Grant ATM-93-01000.
 75. National Science Foundation, Grant ATM-93-01000.
 76. National Science Foundation, Grant ATM-93-01000.
 77. National Science Foundation, Grant ATM-93-01000.
 78. National Science Foundation, Grant ATM-93-01000.
 79. National Science Foundation, Grant ATM-93-01000.
 80. National Science Foundation, Grant ATM-93-01000.
 81. National Science Foundation, Grant ATM-93-01000.
 82. National Science Foundation, Grant ATM-93-01000.
 83. National Science Foundation, Grant ATM-93-01000.
 84. National Science Foundation, Grant ATM-93-01000.
 85. National Science Foundation, Grant ATM-93-01000.
 86. National Science Foundation, Grant ATM-93-01000.
 87. National Science Foundation, Grant ATM-93-01000.
 88. National Science Foundation, Grant ATM-93-01000.
 89. National Science Foundation, Grant ATM-93-01000.
 90. National Science Foundation, Grant ATM-93-01000.
 91. National Science Foundation, Grant ATM-93-01000.
 92. National Science Foundation, Grant ATM-93-01000.
 93. National Science Foundation, Grant ATM-93-01000.
 94. National Science Foundation, Grant ATM-93-01000.
 95. National Science Foundation, Grant ATM-93-01000.
 96. National Science Foundation, Grant ATM-93-01000.
 97. National Science Foundation, Grant ATM-93-01000.
 98. National Science Foundation, Grant ATM-93-01000.
 99. National Science Foundation, Grant ATM-93-01000.
 100. National Science Foundation, Grant ATM-93-01000.